Triplet Electron Transfer and Spin Polarization in a Palladium Porphyrin–Fullerene Conjugate

Journal:	*Physical Chemistry Chemical Physics*
Manuscript ID	CP-ART-08-2018-004937.R2
Article Type:	Paper
Date Submitted by the Author:	17-Oct-2018
Complete List of Authors:	Poddutoori, Prashanth; University of Minnesota Duluth, Chemistry&Biochemistry Kandrashkin, Yuri; Zavoisky Physical -Technical Institute, Obondi, Chris; University of North Texas, Department of Chemistry DSouza, Francis; University of North Texas, Department of Chemistry van der Est, Art; Brock University, Chemistry

SCHOLARONE™
Manuscripts

PCCP

PAPER

Triplet Electron Transfer and Spin Polarization in a Palladium Porphyrin–Fullerene Conjugate

Received 00th January 20xx,
Accepted 00th January 20xx

DOI: 10.1039/x0xx00000x

www.rsc.org/

Prashanth K. Poddutoori,[a] Yuri E. Kandrashkin,[b] Christopher O. Obondi,[c] Francis D'Souza,[c] and Art van der Est *[d]

Transient electron paramagnetic resonance (TREPR) spectroscopy is used to investigate the pathway and dynamics of electron transfer in a palladium porphyrin-fullerene donor-acceptor conjugate. The heavy Pd atom in the porphyrin greatly enhances the rate of intersystem crossing and as a result, electron transfer from the porphyrin to fullerene occurs via the porphyrin triplet state. The sign of the polarization pattern of the radical pair generated by the electron transfer is opposite in benzonitrile and the liquid crystal 5CB. This difference is the result of a change in sign of the spin-spin coupling, which allows the values of the dipolar and exchange couplings between the electrons in the charge-separated state to be estimated. In addition to the radical pair, signals from the fullerene triplet state are also observed. The polarization of the fullerene triplet state inverts with time, while the radical pair signal decays to a multiplet pattern that persists for times longer than the spin-lattice relaxation time. A kinetic model, developed to explain these effects, reveals that forward and reverse electron transfer between the charge-separated state and the fullerene takes place. This process, combined with singlet recombination of the radical pair accounts for the inversion of the fullerene triplet state polarization and the long-lived multiplet polarization of the radical pair.

Introduction

Donor-acceptor dyads and triads have been studied widely as models for the electron transfer (ET) co-factors in photosynthetic reaction centres[1, 2] and for their potential use in photonics devices[3]. The main goal of most of these studies has been to better understand the principles governing the quantum yield, rate and overall energy efficiency of the charge separation. The challenge is to find ways of obtaining a high quantum yield of ET, while minimizing the energy losses and maintaining the charge separation for as long as possible. Such studies have shown that control of the reorganization energy, λ, is crucial and that the quantum yield can be greatly improved by using acceptors such as C_{60}[4] or liquid crystalline solvents[5, 6] to reduce λ. Many other factors such as the charge-transfer nature of the initial excitation[7], nature of the bridging groups between the donor and acceptor[8] and the distance between the donor and acceptor have also been studied. Considerably less attention has been paid to the role of spin in the ET process. This is largely because the initial excitation is usually to the excited singlet state and intersystem crossing (ISC) is seen as a pathway to be avoided because of the energy loss involved. Triplet states can also react with oxygen and result in reactive oxygen species that may be detrimental to the long-term stability of the complex. However, recently we have shown that introducing palladium into a porphyrin-fullerene dyad (Figure 1) to promote fast ISC also results in a greater yield of ET and storage of a larger fraction of the photon energy[9]. This is because the long lifetime of the porphyrin triplet state allows the rate of ET to be lower. Thus, the donor and acceptor can be placed at a larger separation and less driving force is required.

The light-induced electron spin polarization associated with fast ET provides an important observable that can reveal details of the process that are otherwise difficult to detect[10]. The polarization can be measured using transient EPR spectroscopy (TREPR), which is a useful complement to optical methods. Although the response time of most TREPR instruments is limited to ~50 ns the polarization patterns can reveal the pathway by which an observed state was populated. The singlet-triplet mixing that occurs during sequential ET can also be used to determine properties of short-lived precursor radical pairs, even when they cannot be detected directly[11-13]. Transient EPR is particularly useful for studying light-induced

[a] Department of Chemistry and Biochemistry, University of Minnesota Duluth, 1039 University Drive, Duluth, MN 55812, USA.
[b] Zavoisky Physical-Technical Institute, FRC Kazan Scientific Center of RAS, Sibirsky Tract 10/7, Kazan 420029, Russian Federation.
[c] Department of Chemistry, University of North Texas, 1155 Union Circle, #305070, Denton, TX 76203-5017, USA.
[d] Department of Chemistry, Brock University, 1812 Sir Isaac Brock Way, St. Catharines, Ontario, L2S 3A1, Canada. Email: avde@brocku.ca

See DOI: 10.1039/x0xx00000x

This journal is © The Royal Society of Chemistry 2018

ET in strongly scattering samples such as solids or ordered liquid, which are difficult to measure using optical methods. Here, we present an analysis of the spin polarization patterns of the Pd containing dyad $(TPA)_3PPd$-C_{60} (see Figure 1) in a liquid crystalline solvent. The results confirm that the radical pair $[(TPA)_3PPd]^{+}\cdot C_{60}^{-}\cdot$ is formed by ET from the triplet state of $(TPA)_3PPd$. In addition a small amount of the fullerene triplet state ($^3C_{60}$) is formed by direct excitation of the fullerene and subsequent intersystem crossing. Forward and reverse ET between $^3C_{60}$ and $[(TPA)_3PPd]^{+}\cdot C_{60}^{-}\cdot$ then results in inversion of the triplet state polarization pattern and creates long-lived multiplet polarization in the charge-separated state. Comparison of the spectra obtained in the liquid crystal with those obtained in an isotropic solvent also allows the sign of the weak exchange coupling between the donor and acceptor to be determined and its magnitude to be estimated. Despite the small value of the electronic coupling, a high yield of charge separation is achieved because the porphyrin triplet state lifetime is long, which allows sufficient time for ET to occur. The weak coupling in turn leads to a comparatively long lifetime of the charge separation.

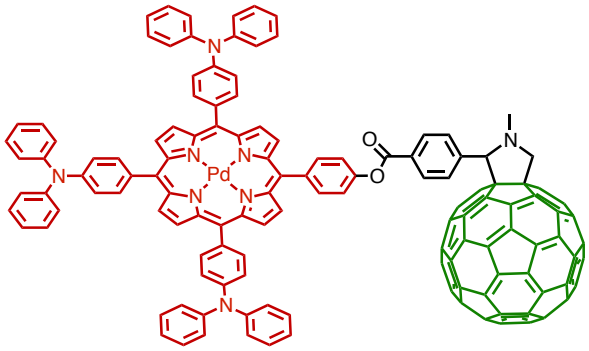

Figure 1. Structure of the palladium(II) porphyrin-fullerene donor-acceptor conjugate $(TPA)_3PPd$-C_{60}.

Materials and Methods

The details of the synthesis and characterization of $(TPA)_3PPd$-C_{60} have been reported elsewhere[9]. Briefly, 5-(4′-hydroxyphenyl)-10, 15, 20-tris (triphenylamino) porphyrin was prepared by condensation of pyrrole with stoichiometric amounts of 4-hydroxybenzaldehyde and 4-diphenylamino-benzaldehyde. The purified porphyrin was then reacted with 4-carboxybenzaldehyde to obtain the ester-linked benzaldehyde porphyrin derivative. Palladium insertion into the porphyrin was then performed by refluxing in the presence of palladium acetate. Finally, the fullerene was attached by reaction with the benzaldehyde functionalized porphyrin and N-methylglycine (sarcosine).

EPR samples were prepared by dissolving the solid porphyrin-fullerene dyad in either benzonitrile (PhCN) or 4′-pentyl-4-biphenylcarbonitrile (5CB) to a nominal concentration of ~1 mM. The PhCN solution was warmed to about 60°C and filtered to remove any undissolved compound and purged with N_2 and placed in a flat cell, which was sealed to prevent contact with oxygen. The 5CB sample was placed in a 4 mm O.D. quartz tube and degassed by repeated freeze-pump-thaw cycles. The modified Bruker EPR 200D-SRC X-band spectrometer used for the TREPR experiments is described elsewhere[14]. The sample was irradiated at 532 nm with 5 ns pulses of a frequency doubled Continuum Surelite I-10 YAG laser. No polarization of the laser beam could be detected at the entrance to the EPR cavity. For the low-temperature measurements, the 5CB sample was placed in the EPR cavity in the cryostat at room temperature and slowly cooled to 80 K in the presence of the magnetic field (~300 mT).

Results and Discussion

The energy level diagram and major relaxation pathways for $(TPA)_3PPd$-C_{60} in PhCN are shown in Figure. 2. The energies of the states have been derived from electrochemical data and the absorption and emission wavelengths of the complex[9]. The relaxation pathways have been determined by femtosecond and nanosecond transient absorbance measurements and TREPR data. Following excitation of the porphyrin very rapid intersystem crossing (ISC) and relaxation to its lowest excited triplet state occurs within 10 ps because of the heavy Pd atom. ET from $^3[(TPA)_3PPd]$ to C_{60} then occurs on a timescale of tens of nanoseconds. Excitation of C_{60} also takes place but because of its low extinction coefficient in the visible region this is a minor process. ISC in C_{60} results in population of its triplet state. The energies of $^3C_{60}$ and $[(TPA)_3PPd]^{\cdot+}$-$C_{60}^{\cdot-}$ are similar and triplet recombination of the radical pair and triplet ET are possible. In PhCN, the optical data did not show any evidence for these processes, thus, it was concluded that the radical pair state lies below $^3C_{60}$ at an energy that makes triplet recombination unfavourable. In 5CB, $[(TPA)_3PPd]^{\cdot+}$-$C_{60}^{\cdot-}$ is expected to be less stabile than in PhCN and the EPR data, which we will present below, suggest that reversible ET between $[(TPA)_3PPd]^{\cdot+}$-$C_{60}^{\cdot-}$ and $^3C_{60}$ occurs. This is shown in blue in Figure 2.

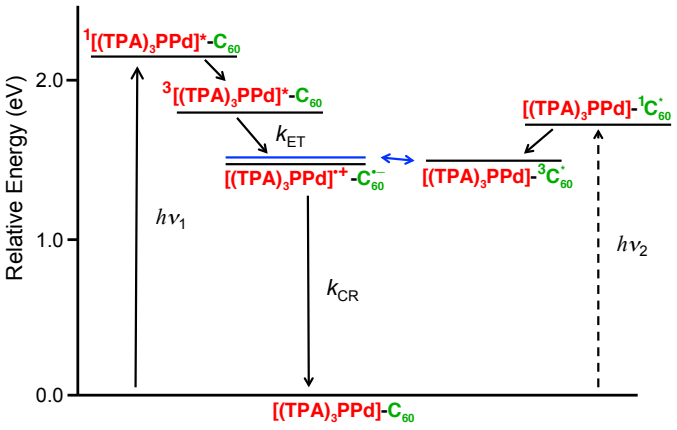

Figure 2. Jablonski diagram showing the main excitation and relaxation pathways of $[(TPA)_3PPd]$–C_{60} in benzonitrile (black arrows and energy levels). The blue energy level and double headed arrow indicate that in 5CB the charge-separated state is destabilized and reversible electron transfer to and from the triplet state of C_{60} occurs. Abbreviations: ISC – intersystem crossing, CR = charge recombination, ET = electron transfer, k = rate. Solid arrow – major process, dashed arrow – minor process.

This journal is © The Royal Society of Chemistry 2018

Figure 3, shows the transient EPR spectra of $(TPA)_3PPd$-C_{60} in 5CB (left) and PhCN (right). Note that the field range for the spectra in 5CB is wider than for those in PhCN. The spectra are plotted such that negative signals are emission (E) and positive signals are absorption (A). As can be seen, the spectra taken in 5CB contain two components. At 20 ns after the laser flash an A/E pattern approximately 5 mT wide is observed, which inverts to E/A at later time (550 ns). In addition, a strong A/E pattern is observed in the center of the spectrum. At 550 ns after the laser flash extremely weak, broad features with A/E polarization and maxima at ~344 mT and ~355 mT is also seen. These features are much longer lived than the rest of the spectrum and are probably due to either an impurity in the sample or a background artifact.

The spectra in PhCN (Figure 3, right) have been reported previously[9] and arise from overlapping contributions from the radical pair $[(TPA)_3PPd]^{\cdot+}$-$C_{60}^{\cdot-}$ and the triplet state of C_{60}. The triplet state of Pd porphryin cannot be observed at X-band because the strong spin-orbit coupling that leads to fast ISC also results in ZFS on the order of ~25 GHz[15], which is larger than Zeeman interaction at X-band making the triplet state undetectable. At 30 ns the weak absorptive spectrum (Figure 3, top right) is mostly due to $^3C_{60}$. At 185 ns the spectrum is dominated by the E/A/E/A polarization pattern of the radical pair $[(TPA)_3PPd]^{\cdot+}$-$C_{60}^{\cdot-}$ that then decays to a weak absorptive signal at late time. The $^3C_{60}$ contribution is purely absorptive at all time points. The overall net absorption in the spectrum is due to the $^3C_{60}$ contribution, while the radical pair contribution has equal amounts of emission and absorption (multiplet polarization). The lack of net polarization in the radical pair is because it is created by ET from the triplet state of $(TPA)_3PPd$. Hence the spin states of the radical pair are populated according to their triplet character which results in pure multiplet polarization.

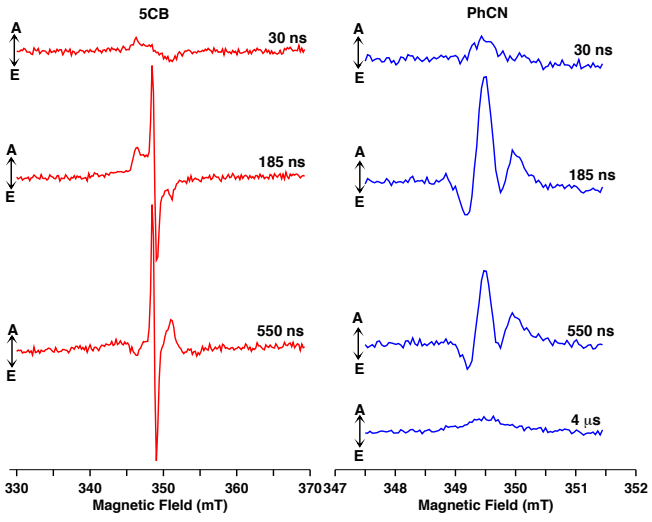

Figure 3. Transient EPR spectra of $[(TPA)_3PPd]$-C_{60} in 5CB (left) and PhCN (right) taken at room temperature.

For the spectra in 5CB, the narrow A/E contribution can be tentatively assigned to the radical pair $[(TPA)_3PPd]^{\cdot+}$-$C_{60}^{\cdot-}$, while the weaker peaks are likely from $^3C_{60}$ and show multiplet polarization because the zero field splitting is not averaged to zero in the liquid crystal. However, several features of the spectra warrant further investigation. First, it is not immediately obvious why the polarization patterns of the radical pair are different in the two solvents. Second, the assignment of the wider, weak A/E pattern needs to be confirmed by comparison with the expected ZFS parameters and ordering of the complex. Finally, the origin of the inversion of the polarization from an A/E pattern to E/A at later time needs to be explained.

We can address some of these questions using the structural model of the complex shown in Figure 4, which was constructed using the program Avogadro[16] and optimized using the UFF force field[17]. As described in detail in the Appendix, the order parameters of the complex can be estimated from its structure using a simple model developed by Samulski, which relates the ordering to the principal moments of inertia[18-20]. The model predicts the largest order parameter S_{cc} to be ~0.66 and the predicted orientation of the principal axes of the order tensor *a, b* and *c* is shown in Figure 4. The description of the ordering can be tested using the low temperature spectra of the complex. Below the freezing point of the liquid crystal, the electron transfer is blocked and only the triplet state of C_{60} is observed. With the ZFS tensor axes oriented as shown in Figure 4 with the Z-axis parallel to the fullerene symmetry axis, the model correctly predicts the orientation dependence of the $^3C_{60}$ spectrum. (see Appendix).

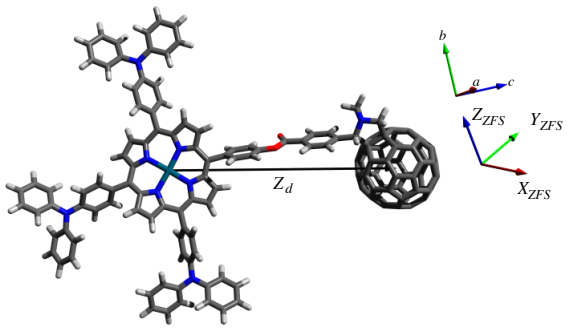

Figure 4. Structural model of $(TPA)_3PPd$-C_{60} showing the principal axes, of the order matrix (*a*, *b*, *c*) and the C_{60} triplet state zero-field splitting tensor (X_{ZFS}, Y_{ZFS}, Z_{ZFS}). The principal axis, Z_d, of the dipolar coupling in the radical pair $[(TPA)_3PPd]^{\cdot+}$–$C_{60}^{\cdot-}$ is also shown.

From the model and the parameters obtained by simulating the low temperature spectra, we can then make a rough prediction of the expected $^3C_{60}$ spectrum at room temperature. In the limit of rapid anisotropic motion the spectrum consists of two peaks separated by $2D_{av}$ where $D_{av} = DS_{zz} + E(S_{xx} - S_{yy})$ and S_{xx}, S_{yy}, S_{zz} are the order parameters of the principal axes of the ZFS tensor. These can be calculated from the principal order parameters of the complex and the Euler angles given in the Appendix. From these values we obtain D_{av} = 67.3 MHz, which corresponds to a predicted splitting of 4.81 mT. Although this prediction is just a

rough estimate it agrees very well with the observed splitting of 4.77 mT for the outer peaks in the room temperature spectra indicating that they do indeed arise from the C_{60} triplet state.

The spectrum of the radical pair can be calculated in a similar manner, using the structure and order parameters to obtain the dipolar coupling. The *g*-factors of the two radicals can be estimated using literature values. For $C_{60}{\cdot}^{-}$ the g-anisotropy is small and we have used the isotropic value given by Zoleo et al.[21] for monofulleropyrrolidine. For $[(TPA)_3PPd]{\cdot}^{+}$ literature values for the g-factors are not available. However, a value of g_{zz} = 1.97 has been reported for the triplet state of a Pd porphyrin[22] and a value of g_{iso} = 1.9975 is obtained from the simulation of the radical pair spectrum in PhCN. The *g*-factor in 5CB is the anisotropic average determined by the order parameters. However, because the principal values of the *g*-tensor are not known, the *g*-factor in 5CB cannot be calculated from the available information. Thus, we have reasoned that it should be close to g_{iso} and adjusted this value slightly so that the positions of the features in the simulated spectra match the observed radical pair spectrum. The exchange coupling is taken from the simulation of the radical pair spectrum in PhCN[9] and is an order of magnitude estimate. These parameters are summarized in Table 1.

Table 1 $[(TPA)_3PPd]{\cdot}^{+}$-$C_{60}{\cdot}^{-}$ Parameters in 5CB

Parameter	Value
spin-spin coupling	d_{eff} = –0.28 mT J = 0.1 mT
g-values	$g([(TPA)_3PPd]{\cdot}^{+})$ = 1.999 $g(C_{60}{\cdot}^{-})$ = 2.00016
linewidths	$\Delta B([(TPA)_3PPd]{\cdot}^{+})$ = 0.4 mT $\Delta B(C_{60}{\cdot}^{-})$ = 0.2 mT

Figure 5 shows the results of the simulations of the TREPR spectra in 5CB at different delay times. The simulated spectra are a weighted sum of the four contributions shown on the left of Figure 6. Since any spin polarization pattern can be divided into a sum of net and multiplet contributions, we have fit the experimental spectra with net and multiplet polarization patterns of the radical pair (Figure 6 upper two spectra) and $^3C_{60}$ (Figure 6 lower two spectra). The right panel of Figure 6 shows the amplitudes of these four contributions as a function of time obtained by fitting them to the spectrum at each time point. As can be seen in Figure 5, good agreement with the experimental spectra is obtained at the different time points shown. The sign of the multiplet polarization A/E corresponds to population of the eigenstates of the radical pair according to their triplet character. The simulations reveal that the reason for the different polarization patterns in PhCN and 5CB is the orientational averaging of the spin-spin interactions. The dipolar coupling is averaged to zero in PhCN whereas in 5CB it is larger than the exchange coupling. Because the two couplings have opposite sign and the magnitude of the dipolar coupling is larger than the exchange coupling, the sign of the overall spin-spin coupling is opposite in the two solvents. Thus, in PhCN the E/A/E/A pattern of a weakly coupling spin pair with positive spin-spin coupling and a triplet precursor is observed. In 5CB, the A/E pattern of a radical pair with moderately strong, negative spin-spin coupling and a triplet precursor is seen.

The fitted coefficients (Figure 6 right) reveal that the radical pair spectrum does not have net polarization (Figure 6 black time trace). The multiplet polarization of the radical pair is strong (Figure 6, red time trace), decaying within ~1 μs to a nearly constant value to the end of the measurement window at 4 μs. For the $^3C_{60}$ contribution, the net polarization (Figure 6, blue trace) is absorptive and rises with a time constant of ~200 ns and then remains essentially constant. The multiplet polarization (Figure 6, green trace) is positive at early time, which corresponds to an A/E pattern and then inverts to an E/A pattern.

The fitted spectra in Figure 5 and the time traces in Figure 6 reveal several interesting aspects of the system and its spin polarization. The most obvious of these is the inversion of the multiplet polarization of the C_{60} triplet. The positive sign of the averaged zero-field splitting, estimated from the simulation of the low temperature spectrum, means that the initial polarization (A/E) corresponds to excess population in the T_0 sublevel. Hence, the inversion of the pattern means that at later time the T_+ and T_- sublevels have greater population. The fast rise time and polarization pattern of the C_{60} triplet indicate that it is formed initially by intersystem crossing. Because the radical pair spectrum rises more slowly than the C_{60} triplet, it does not make a significant contribution at very early time (Figures 3 and 5, top spectra) but at later times, it is the largest contribution.

This journal is © The Royal Society of Chemistry 2018

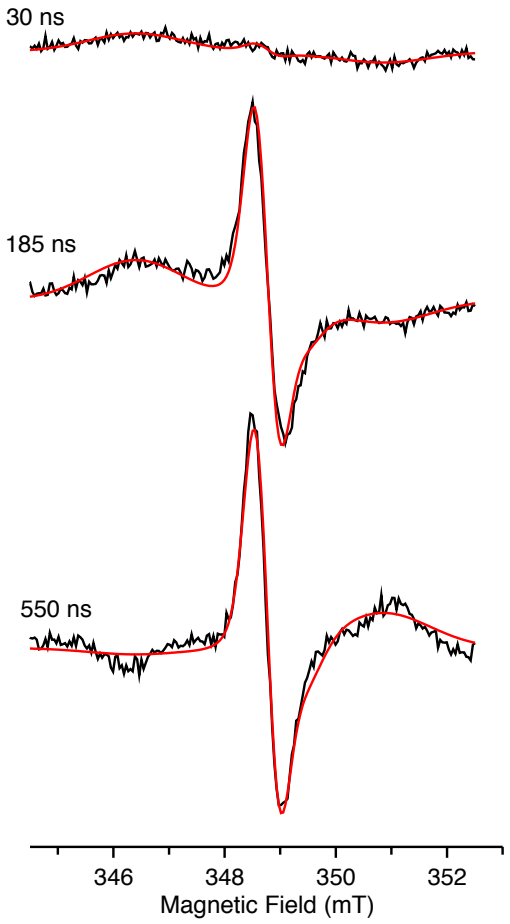

Figure 5. Simulation of the TREPR spectra of $(TPA)_3PPd\text{-}C_{60}$ in 5CB at room temperature. The experimental spectra (black) are the average signal in a 20 ns wide time window centered at the time indicated beside the trace. The simulated spectra are shown in red.

Nanosecond transient absorbance data reported previously[9] show that ET from the $(TPA)_3PPd$ triplet state occurs on a timescale of several tens of nanoseconds, which is consistent with the rise time observed here. The inversion of the triplet polarization can be understood as arising from triplet recombination of the radical pair. Because the T_+ and T_- states of the radical pair do not mix with the singlet state, triplet recombination from these states is faster than from the two sublevels with mixed S,T_0 character. Thus, during the recombination to $^3C_{60}$, the population of its T_+ and T_- sublevels will increase relative to the population of the T_0 level. In the absence of spin relaxation or decay to the ground state, the polarization of the triplet state arising from this selectivity will be transient. The selective recombination should also lead to inversion of the population in the radical pair, since triplet ET preferentially populates the T_+ and T_- sublevels and triplet recombination preferentially depopulates them. However, the sign of the polarization of the radical pair does not invert and A/E polarization is observed to the end of the time window of the collected data. Thus, we can conclude that spin relaxation and/or decay to the ground state also play a role. The initial decay of the radical pair polarization suggests that T_1 relaxation occurs on a time scale of ~1 μs. Nonetheless the multiplet polarization persists for much longer. This effect can be explained as a result of depopulation of the radical pair states with singlet character by recombination to the singlet ground state.

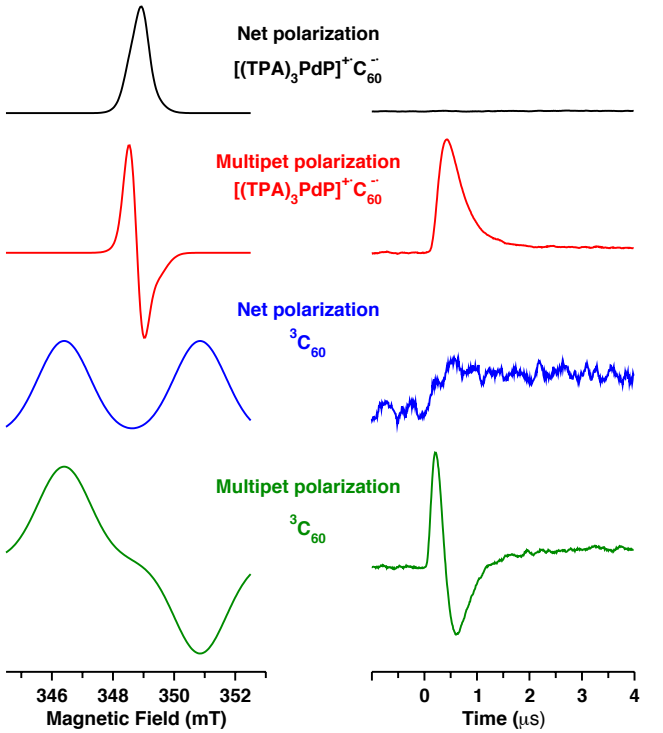

Figure 6. Contributions to the simulated TREPR spectra of $(TPA)_3PPd\text{-}C_{60}$ 5CB at room temperature (left) and their time dependence (right) obtained by a global fit of the time/field dataset. The spectra (left) have been normalized to give the same maximum absorptive amplitude. The time traces associated with $^3C_{60}$ (blue and green) have been scaled by a factor of 9 to account for the estimated relative yields of $[(TPA)_3PPd]^+\text{-}C_{60}^-$ and $^3C_{60}$ generated by the light excitation.

Figure 7 shows a schematic representation of the proposed development of the spin state populations at different times after the laser flash. At early time, (panel A) a small amount of $^3C_{60}$ is generated by ISC, which populates primarily the T_0 sublevel. As ET from $^3[(TPA)_3PPd]$ occurs (panel B) the spin sublevels of the radical pair are populated according to their triplet character, which leads to higher population of the states ψ_1 and ψ_4, which are pure triplet states (see Equation (1)). Subsequently, forward and reverse ET with $^3C_{60}$ leads to inversion of the population distribution in the $^3C_{60}$ spin states (panel C). Finally, at long times (panel D) T_1 relaxation and the forward and reverse ET leads to equilibration of the populations while singlet recombination from the states ψ_2 and ψ_3 of the radical pair maintains weak multiplet polarization.

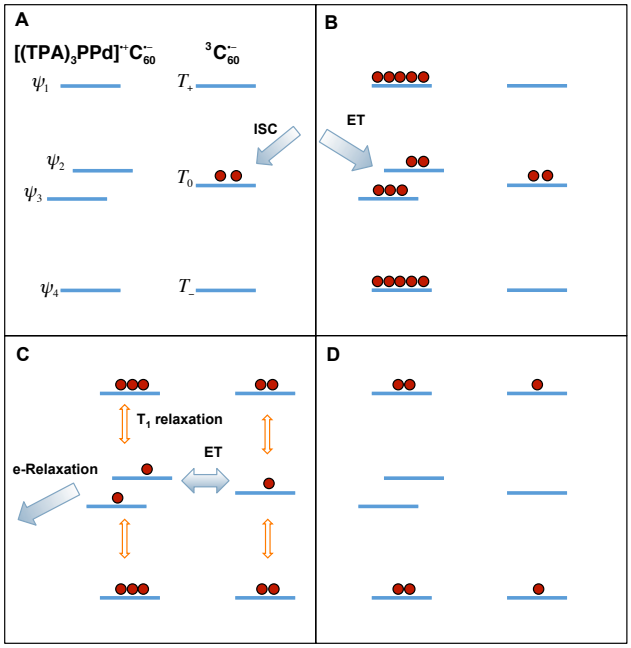

Figure 7 Qualitative representation of the spin state populations at different times. A: ~30 ns after the laser flash. $^3C_{60}$ is populated by intersystem crossing B: ~50-200 ns after the laser $[(TPA)_3PPd]^{+}\cdot C_{60}^{-}\cdot$ is populated by ET from $^3[(TPA)_3PPd]$ C: ~500 ns forward and reverse ET between $[(TPA)_3PPd]^{+}\cdot C_{60}^{-}\cdot$ and $^3C_{60}$ leads to inversion of the population distribution in $^3C_{60}$. D: > 1 μs the combination of forward and reverse ET along with singlet recombination maintains multiplet polarization for times longer than the T_1 relaxation time.

To test this description we have calculated the evolution of the spin state populations using a kinetic model. For both $[(TPA)_3PPd]^{+}\cdot C_{60}^{-}\cdot$ and $^3C_{60}$ we use the wavefunctions:

$$\begin{aligned}\psi_1 &= \left|T_+\right\rangle \\ \psi_2 &= \cos\phi\left|S\right\rangle + \sin\phi\left|T_0\right\rangle \\ \psi_3 &= -\sin\phi\left|S\right\rangle + \cos\phi\left|T_0\right\rangle \\ \psi_4 &= \left|T_-\right\rangle\end{aligned} \tag{1}$$

For $[(TPA)_3PPd]^{+}\cdot C_{60}^{-}\cdot$, the simulation of the radical pair spectrum gives ϕ = 0.54 radians. For $^3C_{60}$ ϕ = 0. We assume that ET between $[(TPA)_3PPd]^{+}\cdot C_{60}^{-}\cdot$ and $^3C_{60}$ conserves the *z*-projection of the spin. Thus, the probability of ET occurring from an initial state $\left|\psi_i\right\rangle$ to a final state $\left|\psi_f\right\rangle$ is $w_{if} = \left|\left\langle\psi_i\middle|\psi_f\right\rangle\right|^2$.

In addition, we assume that the coherence created by the ET decays rapidly and can be ignored. This leads to the following kinetic equations for the evolution of the populations of the RP and triplet states as a result ET between $[(TPA)_3PPd]^{+}\cdot C_{60}^{-}\cdot$ and $^3C_{60}$:

$$\begin{aligned}\dot{n}_{T,i} &= -R(n_{T,i}) - k_+ n_{T,i}\sum_f w_{if} + k_-\sum_f w_{if} n_{RP,f} \\ \dot{n}_{RP,i} &= -R(n_{RP,i}) - k_- n_{RP,i}\sum_f w_{if} + k_+\sum_f w_{if} n_{T,f}\end{aligned} \tag{2}$$

where k_- is the rate of triplet recombination of the radical pair and k_+ is the rate of radical pair formation from $^3C_{60}$. The indices *i* and *f* refer to the four states in Equation (1) and *T* and *RP* refer to $^3C_{60}$ and $[(TPA)_3PPd]^{+}\cdot C_{60}^{-}\cdot$, respectively. The excited singlet state of C_{60} (ψ_2 with ϕ = 0) is assumed to be much higher in energy than the other states and therefore is not involved in the ET processes. The terms $R(n_{T,i})$ and $R(n_{RP,i})$ describe the spin-lattice relaxation and are given by:

$$\begin{aligned}R(n_{T,1}) &= (-p_B + n_{T,3} - n_{T,1})/T_T \\ R(n_{T,3}) &= (n_{T,1} + n_{T,4} - 2n_{T,3})/T_T \\ R(n_{T,4}) &= (p_B + n_{T,3} - n_{T,4})/T_T \\ R(n_{RP,1}) &= (-p_B + (n_{RP,2} + n_{RP,3})/2 - n_{RP,1})/T_{RP} \\ R(n_{RP,i=2,3}) &= ((n_{T,1} + n_{T,4})/2 - n_{RP,i})/T_{RP} \\ R(n_{RP,4}) &= (p_B + (n_{RP,2} + n_{RP,3})/2 - n_{RP,4})/T_{RP}\end{aligned} \tag{3}$$

where T_T and T_{RP} are spin-lattice relaxation times and $p_B = g\beta H/kT$ is the thermal (Boltzmann) polarization. Equations (2) and (3) conserve the total population of $[(TPA)_3PPd]^{+}\cdot C_{60}^{-}\cdot$ and $^3C_{60}$ and the stationary solutions $k_+/(4k_+ + 3k_-)$ and $k_-/(4k_+ + 3k_-)$ are obtained for their respective populations, if the small amount of thermal polarization is neglected. When singlet recombination to the ground state is included, the rate equations for the populations of states 2 and 3 of $[(TPA)_3PPd]^{+}\cdot C_{60}^{-}\cdot$ become:

$$\begin{aligned}\dot{n}_{RP,2} &= -R(n_{RP,2}) - k_- n_{RP,2}\sum_f w_{2f} \\ &\quad + k_+\sum_f w_{2f} n_{T,f} - n_{RP,2} k_0 \cos^2\phi \\ \dot{n}_{RP,3} &= -R(n_{RP,3}) - k_- n_{RP,3}\sum_f w_{3f} \\ &\quad + k_+\sum_f w_{3f} n_{T,f} - n_{RP,3} k_0 \sin^2\phi\end{aligned} \tag{4}$$

Equations (2), (3) and (4) can be solved numerically to give the populations of the spin sublevels as a function of time and from these, the net and multiplet contributions to the polarization can be calculated as:

$$\begin{aligned}p_{net,RP} &= (n_{RP,4} - n_{RP,1}) \\ p_{net,T} &= (n_{T,4} - n_{T,1}) \\ p_{mult,RP} &= \tfrac{1}{2}(n_{RP,1} + n_{RP,4}) - \cos^2\phi n_{RP,3} - \sin^2\phi n_{RP,2} \\ p_{mult,T} &= -\left\{\tfrac{1}{2}(n_{T,1} + n_{T,4}) - n_{T,3}\right\}\end{aligned} \tag{5}$$

This journal is © The Royal Society of Chemistry 2018

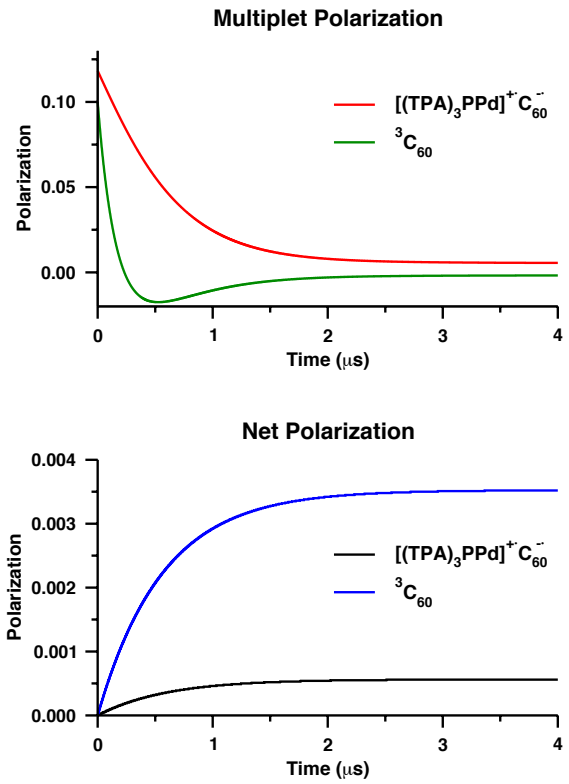

Figure 8 Calculated net and multiplet contributions to the polarization of $[(TPA)_3PPd]^{+\cdot}C_{60}^{-\cdot}$ and $^3C_{60}$. Top panel: multiplet polarization green $^3C_{60}$, red $[(TPA)_3PPd]^{+\cdot}C_{60}^{-\cdot}$. Bottom panel: net polarization, blue $^3C_{60}$, black $[(TPA)_3PPd]^{+\cdot}C_{60}^{-\cdot}$. The parameters used in the calculation are given in the text.

These expressions correspond approximately to the amplitudes of the four components shown in Figure 6. The negative sign of the multiplet polarization of $^3C_{60}$ is to take into account the opposite signs of the spin-spin coupling in $^3C_{60}$ and $[(TPA)_3PPd]^{+\cdot}C_{60}^{-\cdot}$. The spin states of $[(TPA)_3PPd]^{+\cdot}C_{60}^{-\cdot}$ are populated initially according to their triplet character. Thus, their relative populations at t = 0 are $n_{RP,1} = n_{RP,4} = 1$, $n_{RP,2} = \sin^2\phi$, $n_{RP,3} = \cos^2\phi$. ISC predominantly populates the T_0 sublevel of $^3C_{60}$ in $[(TPA)_3PPd]$-C_{60} when it is partially oriented in 5CB. Thus, for $^3C_{60}$ the relative populations at t = 0 are $n_{T,1} = n_{T,4} = 0$, $n_{T,3} = 1$. Finally, we assume that the relative yields of $[(TPA)_3PPd]^{+\cdot}C_{60}^{-\cdot}$ and $^3C_{60}$ are ~90% and ~10% respectively based on the difference in their absorbance at 532 nm and relative contributions to the TREPR spectra. Using, the value of ϕ = 0.54 radians and normalizing to a total radical pair population of 1, we obtain the initial populations: $n_{RP,1}$ = $n_{RP,4}$ = 0.333, $n_{RP,2}$ = 0.088, $n_{RP,3}$ = 0.245, $n_{T,1}$ = $n_{T,4}$ = 0, $n_{T,1}$ = 0.1. The kinetic rate constants have been taken as k_0 = 5 μs^{-1}, k_- = 2 μs^{-1}, k_+ = 0.1 μs^{-1} and the relaxation times as T_T = 0.5 μs and T_{RP} = 3.3 μs. Figure 8 shows the multiplet and net contributions to the polarization (Equation. (5)) calculated using these values. As can be seen, the inversion of the triplet multiplet polarization (Figure 8, green curve) and the long-lived multiplet polarization of $[(TPA)_3PPd]^{+\cdot}C_{60}^{-\cdot}$ (Figure 8, red curve) are both reproduced. Overall, the behaviour is in good qualitative agreement with the experimental curves (Figure 6, right panel).

Conclusions

The analysis above provides a quite detailed picture of the dynamics of the charge separation process in $(TPA)_3PPd$-C_{60}. First, the change in sign of the polarization in PhCN and 5CB shows that the exchange coupling is positive and smaller in magnitude than the dipolar coupling. For most dyads, such small electronic coupling between the donor and acceptor would result in a very poor yield of electron transfer. However, in both PhCN and 5CB, the spin polarization patterns confirm that electron transfer occurs via the triplet state of $(TPA)_3PPd$. Because the porphyrin triplet state is long lived it allows slow electron transfer to occur despite the weak coupling.

In PhCN, nanosecond transient absorbance data[9] show that triplet charge recombination does not occur in this solvent. In contrast, in 5CB inversion of the polarization of $^3C_{60}$ is a clear signature of the triplet recombination. The reason for this difference in the two solvents is likely greater stabilization of charge-separated state in PhCN so that, although it is energetically close to that of the fullerene triplet state, it is far enough below that triplet recombination is not favourable. In 5CB, it appears that the fullerene triplet state and the charge-separated state are very close in energy so that forward and reverse ET can occur. The interesting feature of this process is that it maintains weak multiplet spin polarization of $[(TPA)_3PPd]^{+\cdot}C_{60}^{-\cdot}$ beyond the spin-lattice relaxation time. In contrast, in PhCN in which triplet recombination does not occur, long-lived multiplet polarization is not observed and only weak absorptive polarization is seen at late times. In both solvents, the yield of the charge separation is promoted by the rapid ISC in $(TPA)_3PPd$. Because the resulting triplet state of $(TPA)_3PPd$ is long lived there is more time available for the charge separation to occur. Moreover, the fact that the charge-separated state is generated from a triplet precursor means that spin relaxation and/or singlet-triplet mixing must occur before relaxation to the ground state can take place. However, triplet recombination does not require singlet-triplet mixing. Hence, a crucial feature of systems like this in which ET occurs via the triplet state of the donor is whether or not triplet recombination is energetically favoured.

Appendix

For the analysis of the room temperature TREPR data of $(TPA)_3PPd$-C_{60} we need an estimate of the principal values and axes of the order matrix of the complex. Previous studies have shown that for large molecules, the ordering of solutes is dominated by short range interactions[23]. A number of different empirical models for these interactions have been developed that reveal that the ordering depends on the size and shape of the solute. Further, if the liquid crystal is modeled by a mean field, the strength of the field is roughly the same for a wide range of nematic liquid crystals including 5CB. In the simplest empirical model, developed by Samulski,[18-20] the shape is approximated as an ellipsoid that can be calculated from the inertia tensor. The maximum anisotropy of an ellipsoid is an infinite rod and its order parameter is assumed to be S_{cc} = 1.

The minimum anisotropy is a perfect sphere, which has $S_{cc} = 0$. For intermediate cases, the order parameters are calculated as:

$$S_{cc} = 1 - \frac{(A_a + A_b)}{2A_c}$$
$$S_{aa} = -\frac{1}{2} + \frac{A_a}{A_c} \quad (6)$$
$$S_{bb} = -\frac{1}{2} + \frac{A_b}{2A_c}$$

where $$A_\alpha = \left[(I_{\beta\beta} + I_{\gamma\gamma} - I_{\alpha\alpha})\frac{5}{2m}\right]^{\frac{1}{2}} \quad (7)$$

and $I_{\alpha\alpha}$, $I_{\beta\beta}$ and $I_{\gamma\gamma}$ are the principal moments of inertia chosen such that $I_{bb} \geq I_{aa} \geq I_{cc}$, and m is the mass of the complex. Despite the fact that this model does not explicitly include the solvent-solute interactions, it has been shown to reproduce the order parameters obtained from the deuterium NMR spectra of flexible alkanes in 5CB and other related liquid crystals.[18-20] We have used this model previously to predict the order parameters of porphyrin-based complexes[24, 25]. From the geometry-optimized structure of the dyad, the principal axes of the inertia tensor and order matrix (*a*, *b*, *c*) have been calculated. The principal order parameters are calculated as S_{aa} = –0.43, S_{bb} = –0.23, S_{cc} = 0.66 using equations (6) and (7).

To test whether this estimate of the order parameters and orientation of the principal axes is reasonable, we use the TREPR spectra of $(TPA)_3$PPd-C_{60} at 80 K in 5CB. At this temperature the loss of reorientation of the solvent makes electron transfer energetically unfavorable and hence only the TREPR spectrum of the triplet state of C_{60} formed by intersystem crossing is observed.

Figure 9 shows two spectra of the C_{60} triplet state in $(TPA)_3$PPd-C_{60} at 80 K. The upper spectrum was obtained by freezing the sample from the nematic phase in the presence of the magnetic field of the EPR spectrometer. The lower spectrum was obtained by rotating the frozen sample by ~90°. The red curves are simulations calculated using the Hamiltonian

$$H = \beta \mathbf{S}\cdot\mathbf{g}\cdot\mathbf{B} + \mathbf{S}\cdot\mathbf{D}\cdot\mathbf{S} \quad (8)$$

The parameters used for the simulations are given in Table 2. Most of these parameters have been taken from the literature and adjusted only slightly to fit the observed spectrum. The negative sign of *D*, which means that at zero field the *Z* sub-level is higher in energy than *X* and *Y*, has been chosen in accordance with sign obtained from ENDOR studies of $^3C_{60}$.[26] The principal g-values and zero-field splitting parameters *D* and *E* are derived from those obtained from high-field EPR studies of the triplet states of the other mono-substituted fullerenes.[27] The polarization of the triplet state has been modeled as the sum of two terms[28] describing the axial and rhombic contributions to the traceless density matrix

$$\Delta\rho = \kappa_\parallel \Delta\rho_\parallel + \kappa_\perp \Delta\rho_\perp$$
$$\Delta\rho_\parallel = \tfrac{3}{2}(\cos^2\theta - 1/3)(S_z^2 - \tfrac{1}{3}\vec{S}^2) \quad (9)$$
$$\Delta\rho_\perp = \tfrac{3}{2}\sin^2\theta\cos 2\phi(S_z^2 - \tfrac{1}{3}\vec{S}^2)$$

where θ and ϕ describe the orientation of the magnetic field in the principal axes of the zero-field-splitting tensor and S_z^2 and $\vec{S}^2$ are the spin operators. Previous studies show that intersystem crossing in C_{60} preferentially populates the T_x sublevel.[29] Thus, the spectra have been fitted with $\kappa_\parallel$ = –1.0, $\kappa_\perp$ = –1.0, which corresponds to the population distribution P_x:P_y:P_z = 1:0:0. The order parameters have been calculated using equations (6) and (7), and the orientation of the ZFS principal axes has been adjusted. The orientation obtained (Figure 4) shows that the *Z*-axis is approximately parallel to the C_2 symmetry axis of the fullerene as expected.

Table 2 $^3C_{60}$ Parameters

Parameter	Value
Zero field splitting (MHz)	D = –232, E = –34
g-tensor	g_{xx} = 2.00115 g_{yy} = 2.00115 g_{zz} = 2.00216
Order parameters	S_{aa} = –0.432, S_{bb} = –0.229, S_{cc} = 0.661
Euler angles between order matrix and ZFS tensor	α =11.0, β =112.7, γ = 125.7

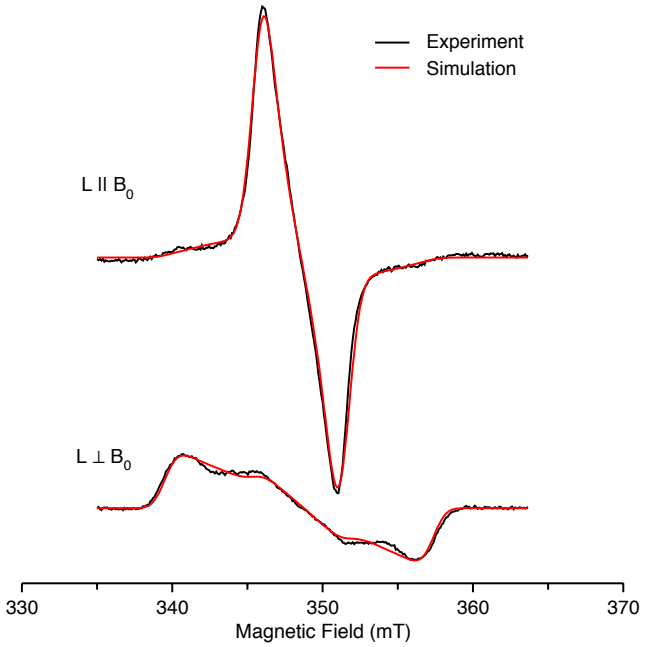

Figure 9. Experimental (black) and simulated (red) spectra of $(TPA)_3$PPd-$^3C_{60}^*$ measured at 80 K in the liquid crystal 5CB. The upper spectrum was measured after freezing the sample from the nematic phase with the director aligned parallel to the field. The lower spectrum was obtained by rotating the frozen sample by ~90º so that the director was perpendicular to the field.

This journal is © The Royal Society of Chemistry 2018

Conflicts of interest

There are no conflicts to declare.

Acknowledgements

This works was supported by a Discovery Grant from NSERC to AvdE and by the University of Minnesota Duluth (startup funds to PKP). Yu.K acknowledges the research program AAAA-A18-118030690040-8 of FRC Kazan Scientific Center of RAS. Support by the US-National Science Foundation (grant no. 1401188 to FD) is acknowledged.

References

1. Y. Tachibana, L. Vayssieres and J. R. Durrant, *Nat. Photonics*, 2012, **6**, 511.
2. B. K. Chandra and F. D'Souza, *Coord. Chem. Rev.*, 2016, **322**, 104-141.
3. B. K. Rugg, B. T. Phelan, N. E. Horwitz, R. M. Young, M. D. Krzyaniak, M. A. Ratner and M. R. Wasielewski, *J. Am. Chem. Soc.*, 2017, **139**, 15660-15663.
4. H. Imahori, H. Yamada, D. M. Guldi, Y. Endo, A. Shimomura, S. Kundu, K. Yamada, T. Okada, Y. Sakata and S. Fukuzumi, *Angew. Chem. Int. Edit.*, 2002, **41**, 2344-2347.
5. G. P. Wiederrecht, W. A. Svec and M. R. Wasielewski, *J. Phys. Chem. B*, 1999, **103**, 1386-1389.
6. G. P. Wiederrecht, W. A. Svec and M. R. Wasielewski, *J. Am. Chem. Soc.*, 1997, **119**, 6199-6200.
7. S. R. Greenfield, W. A. Svec, D. Gosztola and M. R. Wasielewski, *J. Am. Chem. Soc.*, 1996, **118**, 6767-6777.
8. M. Gilbert and B. Albinsson, *Chem. Soc. Rev.*, 2015, **44**, 845-862.
9. C. O. Obondi, G. N. Lim, B. Churchill, P. K. Poddutoori, A. van der Est and F. D'Souza, *Nanoscale*, 2016, **8**, 8333-8344.
10. A. van der Est and P. K. Poddutoori, in *Photosynthesis: Structures, Mechanisms, and Applications*, Springer, 2017, pp. 359-387.
11. Y. E. Kandrashkin, K. Salikhov, A. van der Est and D. Stehlik, *Appl. Magn. Reson.*, 1998, **15**, 417-447.
12. P. K. Poddutoori, G. N. Lim, A. S. Sandanayaka, P. A. Karr, O. Ito, F. D'Souza, M. Pilkington and A. van der Est, *Nanoscale*, 2015, **7**, 12151-12165.
13. P. K. Poddutoori, N. Zarrabi, A. G. Moiseev, R. Gumbau-Brisa, S. Vassiliev and A. van der Est, *Chemistry–A European Journal*, 2013, **19**, 3148-3161.
14. W. Xu, P. Chitnis, A. Valieva, A. van der Est, Y. N. Pushkar, M. Krzystyniak, C. Teutloff, S. G. Zech, R. Bittl and D. Stehlik, *J. Biol. Chem.*, 2003, **278**, 27864-27875.
15. J. Kooter and G. Canters, *Mol. Phys.*, 1980, **41**, 361-375.
16. M. D. Hanwell, D. E. Curtis, D. C. Lonie, T. Vandermeersch, E. Zurek and G. R. Hutchison, *J. Cheminformatics*, 2012, **4**, 17.
17. A. K. Rappé, C. J. Casewit, K. Colwell, W. A. Goddard III and W. Skiff, *J. Am. Chem. Soc.*, 1992, **114**, 10024-10035.
18. E. T. Samulski, *Ferroelectrics*, 1980, **30**, 83-93.
19. E. T. Samulski and R. Y. Dong, *J. Chem. Phys.*, 1982, **77**, 5090-5096.
20. E. T. Samulski and H. Toriumi, *J. Chem. Phys.*, 1983, **79**, 5194-5199.
21. A. Zoleo, A. L. Maniero, M. Prato, M. G. Severin, L. C. Brunel, K. Kordatos and M. Brustolon, *J. Phys. Chem. A*, 2000, **104**, 9853-9863.
22. H. Miwa, K. Ishii and N. Kobayashi, *Chem. Eur. J.*, 2004, **10**, 4422-4435.
23. A. van der Est, M. Kok and E. Burnell, *Mol. Phys.*, 1987, **60**, 397-413.
24. Y. E. Kandrashkin, P. K. Poddutoori and A. van der Est, *Appl. Magn. Reson.*, 2016, **47**, 511-526.
25. A. van der Est, G. Fuechsle, D. Stehlik and M. Wasielewski, *Appl. Magn. Reson.*, 1997, **13**, 317-335.
26. G. Van den Berg, D. Van den Heuvel, O. Poluektov, I. Holleman, G. Meijer and E. Groenen, *J. Magn. Reson.*, 1998, **131**, 39-45.
27. M. Bortolus, M. Prato, J. van Tol and A. L. Maniero, *Chem. Phys. Lett.*, 2004, **398**, 228-234.
28. Y. E. Kandrashkin, P. Poddutoori and A. van der Est, *Appl. Magn. Reson.*, 2006, **30**, 605.
29. X. Dauw, G. Van den Berg, D. Van den Heuvel, O. Poluektov and E. Groenen, *J. Chem. Phys.*, 2000, **112**, 7102-7110.

1

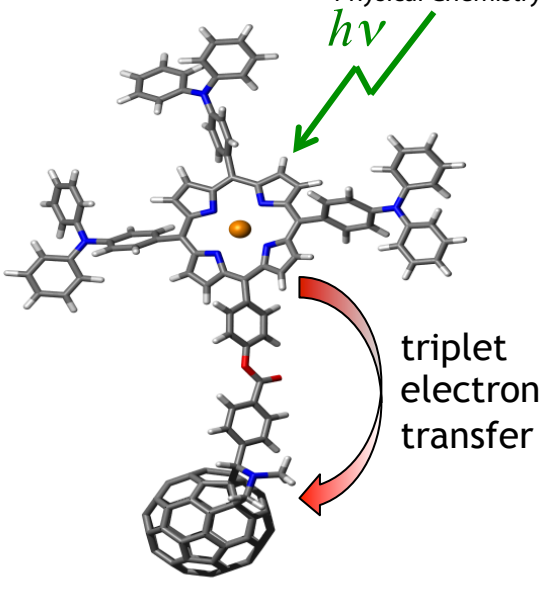
hν
triplet
electron
transfer

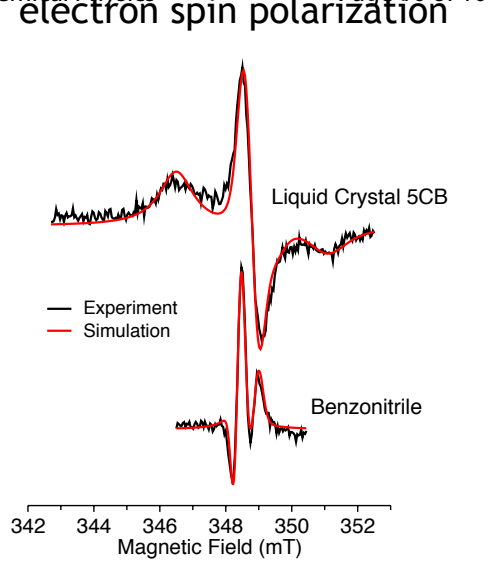
electron spin polarization
Liquid Crystal 5CB
Experiment
Simulation
Benzonitrile
342
344
346
348
350
352
Magnetic Field (mT)